scientific reports

Check for updates

OPEN

The morpho-kinetic landscape of macrophage modes during wound healing in zebrafish

Seol Ah Park[1]✉, Giulia Lupi[1], Resul Ozbilgic[2], Michal Kollár[1], Aneta A. Ožvat[1], Mai Nguyen-Chi[2] & Karol Mikula[1]

Macrophages play an essential role in wound healing due to their dynamic nature and functional plasticity, exhibiting highly heterogeneous morpho-kinetic behaviors depending on their activation states. However, quantitative analysis of macrophage behavior in *in vivo* settings remains limited, largely due to the complexity of their diverse morphologies and motility patterns over time. In this study, we present an analytic workflow to investigate macrophage dynamics in zebrafish. By computing a comprehensive set of morpho-kinetic features, we observe that M1-like (pro-inflammatory) and M2-like (anti-inflammatory) macrophages exhibit distinct behaviors, such as reduced shape elongation, more directed movement, and less random-like motion in M1-like compared to M2-like macrophages. Based on these features, we classify macrophages in the transition period into cM1-like (classified M1-like) and cM2-like (classified M2-like) groups. We compare and analyze their behaviors, which allows us to estimate the timing of the phenotypic switch. In addition, macrophages not expressing Tumor Necrosis Factor (TNF) are located significantly farther from the wound compared to M1-like macrophages. While macrophages unstimulated by wound signaling exhibit some cM2-like features, they differ notably in shape elongation and migration speed. In summary, this study provides a quantitative analysis of macrophage behavior during wound healing and suggests distinct behavioral landscapes across different macrophage activation states.

Wound healing is a fundamental biological process that restores tissue integrity following injury and provides protection against pathogens. Efficient healing is therefore fundamental for maintaining overall health, preventing infections, and reducing healthcare burdens[1]. Among the various immune cells involved in wound healing, macrophages are essential to wound healing, given their dynamic nature and functional plasticity. As key components of the innate immune system, macrophages take on the role of frontline defenders against pathogens and contribute to tissue homeostasis, repair, and the progression of various diseases, including cancer, chronic inflammation, and infections[2].

Traditionally, macrophages in wound healing have been described in two main phases[3]: the early recruitment of pro-inflammatory M1 macrophages, followed by a transition to anti-inflammatory M2 macrophages. M1-like macrophages dominate the initial inflammatory phase, producing cytokines such as Tumor Necrosis Factor (TNF) and Interleukin-6 (IL-6), and exhibiting strong phagocytic activity to clear pathogens and debris[4,5]. As inflammation subsides, macrophages shift toward the M2-like phenotype, supporting tissue repair and resolution through factors like Transforming Growth Factor-β1 (TGF-β1)[6,7]. It has been observed that their polarization state correlates with distinct morphological and migratory features across different model systems[8–11]. In murine models, M1-like macrophages are typically rounded and flattened, while M2-like macrophages are elongated. Correspondingly, studies in human macrophages and monocytes have shown that M1-like cells predominantly use fast, adhesion-independent amoeboid migration, whereas M2-like cells exhibit slower, adhesion-dependent mesenchymal movement[9,12]. However, it has been reported that macrophage activation occurs along a continuum, including intermediate and non-classical phenotypes, shaped by local environmental cues and not strictly conforming to the M1/M2 framework[13–15]. A comprehensive understanding of this spectrum of macrophage modes is therefore crucial, as it provides valuable insights into macrophage functions during tissue repair and helps guide therapeutic strategies for inflammatory and wound healing disorders.

In vivo experiments provide unique opportunities to observe the temporal and spatial dynamics of macrophage plasticity and responsiveness during wound healing, offering valuable insights into their functional dynamics and

[1]Department of Mathematics and Descriptive Geometry, Faculty of Civil Engineering, Slovak University of Technology, Bratislava, Slovak Republic. [2]LPHI, Université de Montpellier, CNRS, INSERM, Montpellier, France. ✉email: seol.park@stuba.sk

regulatory mechanisms. While several studies in zebrafish have quantitatively analyzed macrophage dynamics in *in vivo* settings[16–18], detailed quantitative analysis of the relationship between macrophage activation states and morpho-kinetic changes remains challenging. A major obstacle is the complexity inherent in analyzing macrophages in dynamic *in vivo* environments, where cells exhibit heterogeneous morphologies and diverse motility patterns over time.

In this paper, we investigate various aspects of macrophage behavior *in vivo* using the zebrafish model during wound healing. We examine not only the classical M1-like and M2-like phenotypes but also macrophages that do not express TNF (NonM1-like), unstimulated macrophages (unM), and macrophages in the transitional phase from M1-like to M2-like. To understand the landscape of macrophage behavior, we analyze it from a morpho-kinetic perspective that captures both morphological and dynamic features. This approach has been demonstrated to be effective for characterizing and clustering the behavior of neutrophils and dendritic cells under inflammatory conditions[19]. Each macrophage mode is quantitatively characterized through detailed morpho-kinetic analysis using advanced image processing techniques tailored to capture complex cellular dynamics. These methods include macrophage segmentation and tracking[20], as well as the extraction of directional versus random-like motion[21]. From time-lapse imaging data, we extract morpho-kinetic features that distinguish macrophage behaviors across modes. Additionally, we apply classification methods[22,23] to identify M1-like and M2-like phenotypes specifically during the transition period. This comprehensive analysis reveals key morpho-kinetic features associated with each macrophage mode and elucidates their relationships. We further identify distinguishing characteristics of M1-like and M2-like macrophages during the transition period and estimate the temporal range of the phenotypic shift. Ultimately, this work offers insights into macrophage dynamics during wound healing and establishes a quantitative framework for analyzing macrophage behavior *in vivo*.

Results

Definition of macrophage modes in this study

To investigate macrophage morpho-kinetic behavior during wound healing *in vivo*, we employed the zebrafish larval fin fold amputation model. M1-like macrophages were tracked using the double transgenic line Tg(mfap4:mCherry-F/tnfa:GFP-f), in which all macrophages express a membrane-bound red fluorescent protein, and those expressing TNF, a hallmark of M1 polarization, also express membrane-localized GFP. We previously demonstrated that GFP^+ macrophages in this model express tnfa alongside other M1-associated markers, including tnfb, il6, and il1b, during the early wound response[16]. Although no M2-specific reporter line was available, prior work showed that GFP^+ M1-like macrophages undergo in situ phenotypic conversion into an M2-like state, characterized by expression of tgfb1, ccr2, and cxcr4b during the resolution phase[16]. Transcriptomic profiling further supported the inflammatory nature of early wound macrophages and the reparative profile of later-stage macrophages[24].

Based on these molecular characteristics and temporal contexts, we defined macrophage modes for this study as follows:

- *M1-like (early wound phase)* GFP^+ macrophages present within the first 6 hours post-amputation (hpa)
- *M2-like (late wound/resolution phase)* macrophages emerging after 10.5 hpa, representing cells transitioning from the M1-like state
- *cM1-like* Classified M1-like macrophages (GFP^+) observed during the transition period (6–10.5 hpa)
- *cM2-like* Classified M2-like macrophages (GFP^+) observed during the transition period (6–10.5 hpa)
- *NonM1-like (absence of TNF signaling)* Macrophages lacking GFP expression within the first 6 hpa
- *unM (unstimulated)* Homeostatic macrophages in uninjured larvae (GFP^-)

This GFP-based reporter system enabled continuous tracking of macrophage activation states as they dynamically adapted their roles during wound repair. Live imaging of fin folds was performed using spinning disk microscopy at defined time points, and macrophage behaviors observed in the recordings were annotated according to these six modes.

Comparative analysis of morpho-kinetic behaviors in M1-like and M2-like macrophages

Using annotated microscopy videos of M1-like (up to 6 hours post-amputation, hpa) and M2-like (10.5–16 hpa) macrophages, we compared their morpho-kinetic features (see Materials and methods for details on video annotation and feature extraction). Based on macrophage segmentation, tracking (Fig. 1A), and trajectory smoothing (Fig. 1B), we computed 63 features (see Supplementary Fig. 7) from 55 macrophage trajectories in M1-like videos (totaling 3308 segmented macrophages across all time frames) and 60 trajectories in M2-like videos (totaling 3034 segmented macrophages across all time frames). Across multiple features, M1-like and M2-like macrophages displayed distinct characteristics, including differences in cell morphology, movement directionality, proximity to the wound site, trajectory shapes, and patterns of random-like motion.

Mean circularity of cell shapes per trajectory revealed that M1-like macrophages generally exhibited higher circularity than M2-like macrophages (Fig. 1C, top-left panel), indicating that M2-like macrophages tend to have more elongated and complex shapes. This observation is consistent with previously reported findings[18].

To assess movement directionality, we used the "Tangent Projection Metric" (TPM); a detailed mathematical definition is available in the Supplementary Information. A TPM value closer to 1 indicates movement toward the wound (along the normal vector of the wound line), while a value closer to -1 indicates movement away. We computed TPM for the original trajectories, indicated by the suffix "ori" in the figure. As shown in the top-right panel of Fig. 1C, the mean TPM for most M1-like trajectories was positive, whereas many M2-like trajectories had negative TPM values. The average TPM thus showed a clear difference between the two phenotypes, suggesting that M1-like macrophages exhibit stronger directional migration toward the wound.

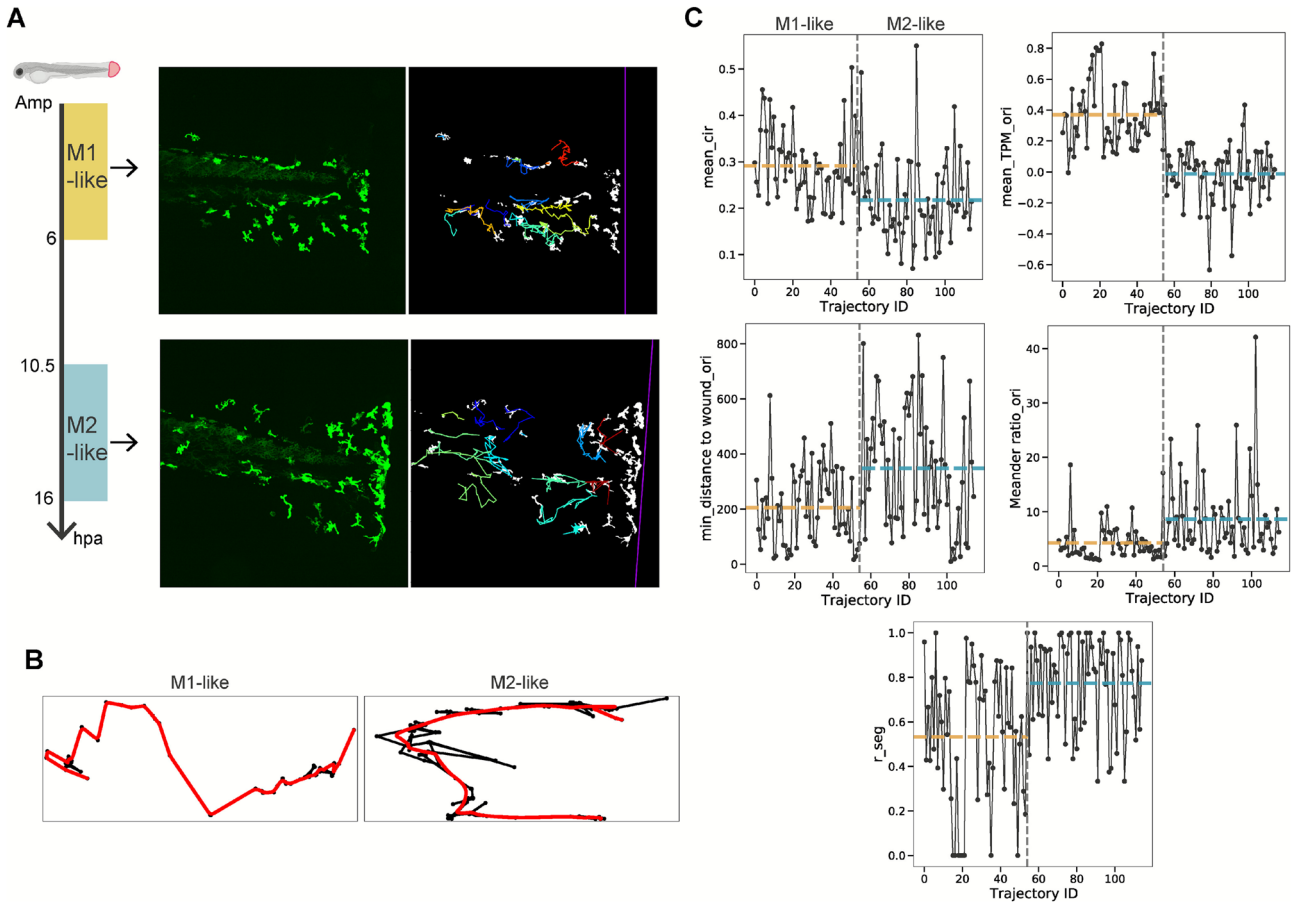

Figure 1. Quantitative analysis of morphology and movement in M1-like vs. M2-like macrophages. (**A**) Examples of macrophage segmentation and tracking from annotated M1-like (GFP^+, 0–6 h post amputation) and M2-like (GFP^+, 10.5–16 post amputation) videos, with vertical violet lines indicating the wound site. The first column shows original images at a single time frame (top: M1-like; bottom: M2-like). The second column shows the results after macrophage segmentation and tracking, where segmented macrophages are displayed in white and individual trajectories are color-coded. (**B**) Smoothed trajectories (red) overlaid on original extracted trajectories (black) from an M1-like (left) and an M2-like (right) trajectory. (**C**) Comparison of features between M1-like and M2-like macrophages: mean circularity of cell shapes (mean_cir), mean Tangent Projection Metric (mean_TPM_ori; positive values indicate movement toward the wound, negative values away from it), minimum distance to the wound (min_distW_ori), meander ratio (M_TPM_ori), and proportion of random-like motion (r_{seg}). For direct comparison, M1-like and M2-like trajectories are presented together. Trajectories from all M1-like videos (55 trajectories total) are shown to the left of the vertical gray dashed line, while trajectories from all M2-like videos (60 trajectories total) are shown to the right. Abbreviations for the feature names are described in detail in the Supplementary Information. The horizontal axis represents macrophage trajectory indices, with M1-like on the left and M2-like on the right of the vertical divider. Dashed yellow and blue lines indicate the average values for M1-like and M2-like, respectively. Features with the "ori" suffix were computed from original (unsmoothed) trajectories.

We also examined how closely macrophages approached the wound. The mean distance can be misleading; for example, when a macrophage moves from a distant location to the wound or vice versa, the resulting average may fall in the mid-range despite the cell having reached the wound. Therefore, we used the minimum distance in each trajectory as a more reliable indicator of wound proximity. In the middle-left panel of Fig. 1C, the minimum distances from the wound site for the original trajectories (indicated by the suffix "ori") are shown for each M1-like and M2-like trajectory. The average minimum distance (dashed lines) was smaller for M1-like macrophages than for M2-like, suggesting that M1-like macrophages are more frequently located near the wound site. Note that although a macrophage that begins near the wound and migrates away would also yield a low minimum distance, this measure still reflects the overall accumulation tendency near the wound.

Trajectory linearity was assessed using the meander ratio, defined mathematically in the Supplementary Information. A value of 1 indicates a perfectly straight path, while higher values reflect increasingly winding trajectories. In the middle-right panel of Fig. 1C, the original trajectories from M1-like showed lower meander ratios than M2-like, implying that M1-like macrophages move in a more directed and linear manner.

Finally, we quantified the portion of each trajectory exhibiting random-like trajectories using the feature, r_{seg}. This measurement quantifies the proportion of time a macrophage spends in random-like motion relative to the total duration of its trajectory. Random-like motion is identified by self-intersections within the trajectory, where the macrophage's path crosses over itself, which can also indicate looping behavior. Higher values suggest that a larger portion of the trajectory involves looping or non-directional movement. As shown in the bottom panel of Fig. 1C, M2-like macrophages had higher values of r_{seg}, indicating that they spent more time in patterns of looping motion. This finding is consistent with the higher meander ratios observed in M2-like macrophages.

Macrophage behavior during the transition period

To investigate macrophage behavior during the transition period (TP), we analyzed videos recorded between 6 and 10.5 hpa. We extracted trajectories from this period and classified them as cM1-like or cM2-like, based on features previously obtained from annotated M1-like and M2-like videos. For classification, we applied a nonlinear graph diffusion-based method[22,23] (see Materials and methods). To optimize the model parameters, we used the feature matrix from the reference M1-like and M2-like datasets (Supplementary Fig. 7) as the training set for the model. The 113 trajectories extracted from the TP, containing 5743 totaling segmented macrophages across all time frames, were then classified by the trained model.

The classification was performed in a reduced feature space, where the original 63 features were projected onto 6 dimensions based on the pattern of the eigenvalue decay from principal component analysis (PCA), as shown in the top panel of Fig. 2A. The bottom-left panel of Fig. 2A shows that PCA of labeled M1-like and M2-like videos results in a largely distinct separation along the first two principal components (PC1-PC2), with some overlap. Interestingly, some trajectories in the TP located in the overlapping region of the PC1-PC2 plane (e.g., the 32^{nd} trajectory, highlighted with a red square) become distinguishable when additional dimensions, such as PC2-PC3 (bottom-right panel of Fig. 2A), are considered. Incorporating additional dimensions improved classification performance, with a training accuracy of 90.4%. As a result, the 113 trajectories from the TP were classified as cM1-like (37 trajectories), cM2-like (75 trajectories), and unclassified (1 trajectory).

Temporal dynamics of several key features were analyzed across the cM1- and cM2-like trajectories (Fig. 2B). Trajectory data were binned into 20-minute intervals, and the mean feature values were calculated for each bin. To ensure statistical robustness, we excluded outliers using the 1.5×IQR criterion and required a minimum average of 12 observations per time frame within each time bin. For instance, a time bin spanning 20 minutes with 2.5-minute sampling intervals contains 8 frames and thus requires $\geq$96 observations (12×8). The top-left panel of Fig. 2B displays the mean TPM, indicating movement directionality relative to the wound. Around 460 minutes post-amputation (mpa), the classified M2-like trajectories begin to exhibit TPM ≤ 0, suggesting reduced migration toward the wound, while cM1-like trajectories maintain directional movement. The top-right panel shows mean distance to the wound, where the cM2-like begin to migrate away from the wound around 550 mpa. In the bottom-left panel, the circularity sharply declines within the same time bin ($\sim$ 550 mpa), suggesting a morphological shift toward more elongated cell shapes. Additionally, cM1-like trajectories exhibit a similar range of speeds during the TP and higher speeds prior to 500 mpa (bottom-right panel). After this time point, cM2-like trajectories exceed them and achieve maximum speed around 550 mpa when active reverse migration begins, followed by a decrease in speed.

To further examine relationships between morpho-kinetic features over time, we generated two-dimensional feature plots for each time bin, represented by semi-transparent points and lines annotated with time bin labels (Fig. 2C). To enhance the visualization of temporal trends, moving averages were calculated using a three-bin sliding window (i.e., averaged over every three consecutive time bins) and are shown as thicker lines in Fig. 2C. The top two panels show that the mean circularity of cM2-like trajectories during the TP begins to decline as they reduce their active migration toward the wound. The bottom two panels show distinct speed patterns between cM1-like and cM2-like macrophages during the TP: cM2-like macrophages accelerate during the phase when active migration to the wound decreases, whereas cM1-like macrophages slow down. Notably, the mean speed of classified cM2-like macrophages appears to be inversely correlated with circularity, as shown in the rightmost panel.

NonM1-like macrophages in comparison with activated M1-like states

The morphologies and trajectories of nonM1-like macrophages, defined as macrophages that do not express the tnfa:GFP-f (green) transgene, were extracted as shown in Fig. 3A (see Materials and methods and Supplementary Fig. 1 for details of the extraction process). We extracted totaling 5266 segmented macrophages across all time frames from 118 trajectories. A total of 63 morpho-kinetic features were computed and projected into PCA planes derived from labeled M1-like and M2-like macrophage data as shown in Fig. 3B. In this PCA plane, many NonM1-like trajectories are positioned closer to the M1-like region, particularly along the PC1-PC2 plane, suggesting that NonM1-like macrophages generally exhibit morpho-kinetic characteristics more similar to M1-like than to M2-like. However, several key features distinguish NonM1-like from activated M1-like macrophages. As shown in Fig. 3C, both M1-like and NonM1-like macrophages migrate toward the wound (similar TPM range); however, NonM1-like macrophages tend to remain at significantly greater distances from the wound site. In terms of morphology, NonM1-like macrophages maintain relatively stable circularity over time, whereas M1-like macrophages become progressively more elongated (lower circularity) as they migrate. Additionally, M1-like macrophages show a gradual increase in speed over time, whereas NonM1-like macrophages accelerate shortly after amputation but slow down later. To explore relationships between features, Fig. 3D shows the two-dimensional plot of mean speed versus circularity for M1-like and NonM1-like macrophages. In general, both modes show an inverse relationship between circularity and speed. In NonM1-like macrophages, circularity tends to decrease as speed increases during the early phase following amputation; however, circularity begins to

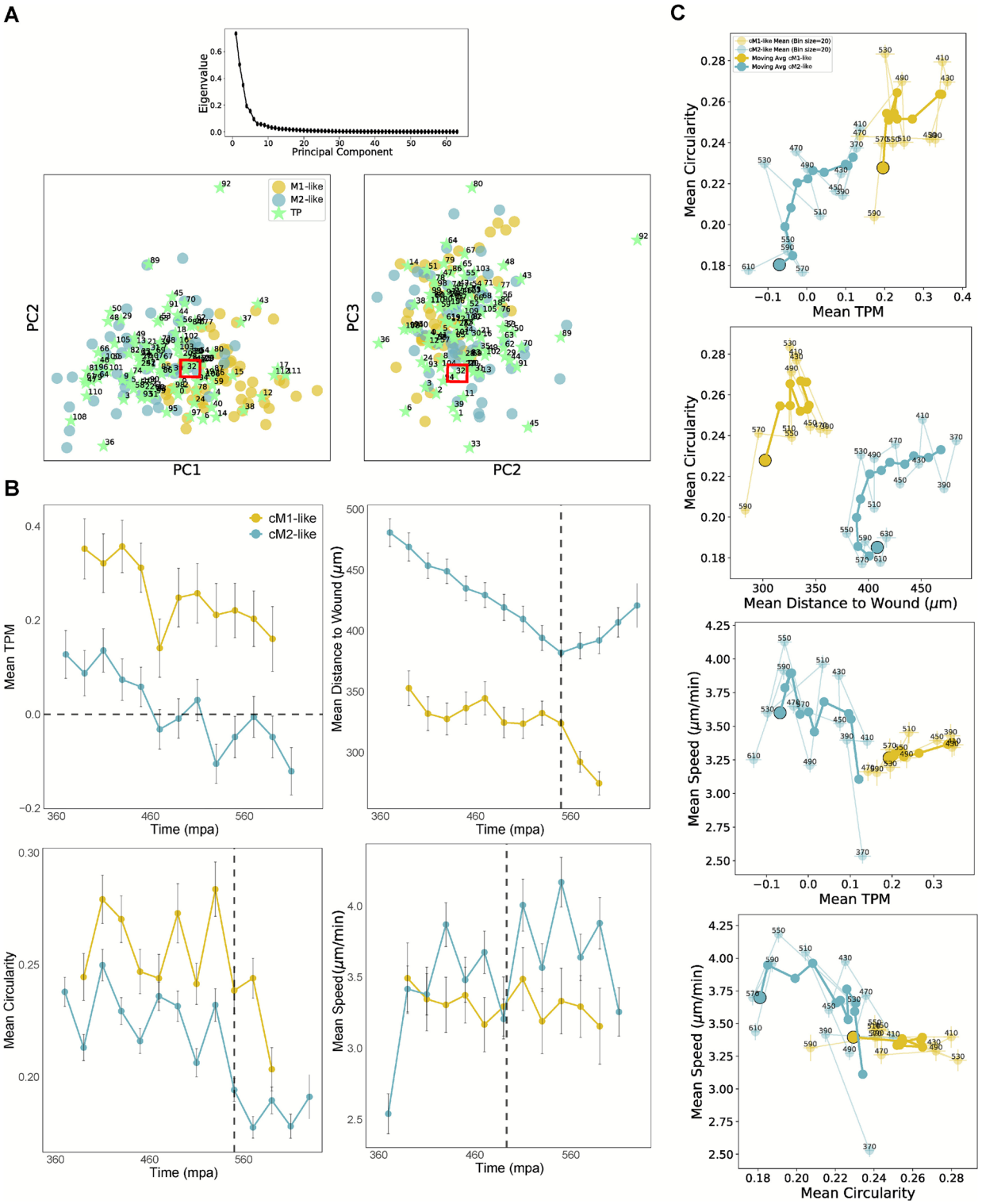

Figure 2. Analysis of macrophage states during the transition period (6–10.5 hours-post-amputation). (**A** PCA-based analysis: eigenvalue decay (top), trajectory projection in PC1-PC2 (bottom-left) and PC2-PC3 (bottom-right) planes. A TP trajectory better separated in PC2-PC3 is marked with a red square (32nd point). (**B**) Temporal trends of key features in cM1-like and cM2-like trajectories from all TP videos, analyzed in 20 min bins: mean TPM (positive values indicate movement toward the wound, negative values away from it), distance to the wound, circularity of cell shapes, and speed. (**C**) Pairwise relationships between features over time, showing mean values for the following pairs: TPM vs. circularity, circularity vs. distance to the wound, TPM vs. speed, and circularity vs. speed. Bold lines represent moving averages using a three-bin sliding window, and annotated numbers indicate the median value of each time bin. The last temporal point of the moving average is marked slightly larger with a black edge.

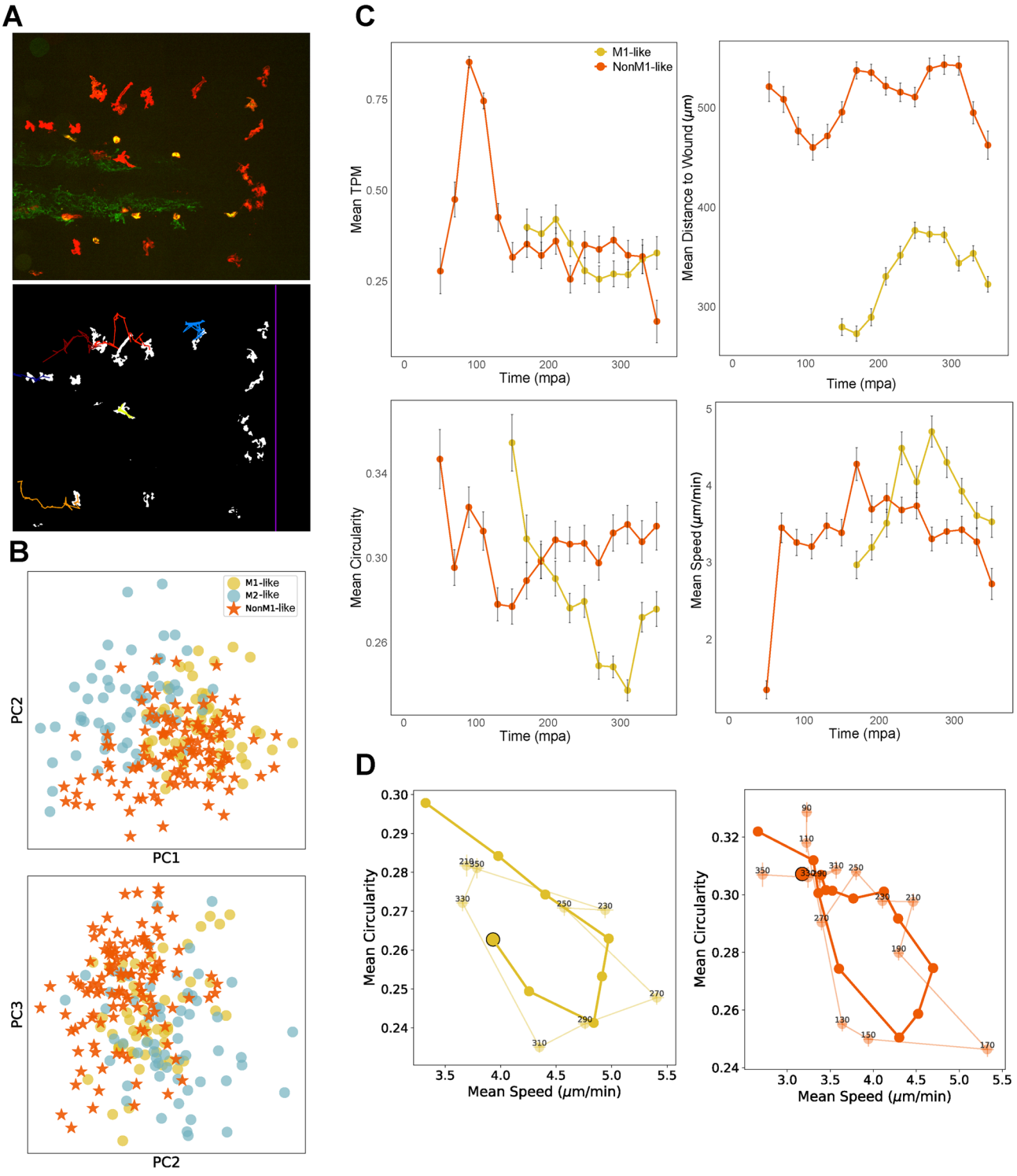

Figure 3. Morpho-kinetic comparison of NonM1-like and M1-like macrophages (0–6 hours-post-amputation) (**A**) Examples of macrophage segmentation and tracking from an annotated NonM1-like video, with vertical violet lines indicating the wound site. The top panel shows an original image at a single time frame (with both red and green channels). The bottom panel shows the result after macrophage segmentation and tracking of NonM1-like macrophages (identified by the absence of green signaling), where segmented macrophages are displayed in white and individual trajectories are color-coded. (**B**) Projection of NonM1-like trajectories onto the PCA planes derived from labeled M1-like and M2-like data. (**C**) Temporal trends of selected features for M1-like and NonM1-like macrophages from all M1-like and NonM1-like videos, analyzed in 20 min bins: mean TPM (top-left; positive values indicate movement toward the wound, negative values away from it), mean distance to the wound (top-right), mean circularity (bottom-left), and mean speed (bottom-right). (**D**) Pairwise feature relationship over time: mean speed versus circularity for M1-like (left) and NonM1-like (right). The last temporal point of the moving average is marked slightly larger with a black edge.

rise around 170 mpa, accompanied by a decrease in speed. In contrast, M1-like macrophages exhibit progressively higher speeds and decreasing circularity over the observed period.

Macrophage behavior in the absence of wound signal

We analyzed the behavior of unM macrophages, defined as macrophages not exposed to a wound signal, from a morpho-kinetic perspective. The steps of video processing were consistent with previous analyses; however, only the mfap4:mCherryF (red) channel was used (top panel of Fig. 4A), since no inflammation was induced therefore the tnfa:GFP-f (green) transgene was not expressed. In these unwounded conditions, macrophages tended to accumulate in specific regions (see Supplementary Fig. 3). For reasonable analysis, we excluded trajectories in which cells remained within such an accumulation zone for more than five consecutive time frames (see bottom panel of Fig. 4A and Materials and Methods for details). As a result, totaling 9917 segmented unM macrophages across all time frames were extracted with 132 trajectories. To compute features related to the wound site, such as movement direction (TPM) and distance to the wound, a reference line corresponding to the site of wound is required. However, since unM macrophages are from unwounded cases, we defined a vertical line closely matching the location of the caudal fin fold to maintain consistency with the wounded condition, as amputations in this study were performed in the caudal fin fold. Using 63 morpho-kinetic features, we projected the unM trajectories onto the PCA planes derived from labeled M1-like and M2-like macrophages. As shown in Fig. 4B, many unM trajectories cluster near the M2-like region in the PC1-PC2 plane, suggesting that unM macrophages share greater similarity with M2-like than with M1-like in terms of overall morpho-kinetic behavior.

In Fig. 4C, the violin plots show the similarities and differences between unM macrophages and other activation states, and also provide a comprehensive overview of the distributional differences across all activation states. In the top-left panel, TPM (computed from original trajectories) for unM is close to zero, and many unM trajectories are distributed near this value, indicating a lack of clear directionality. The median value of mean TPM for unM closely resembles that of M2-like macrophages. However, the M2-like macrophages exhibit a longer tail in the negative TPM range, reflecting the active reverse migration described earlier (see second Results section). In the middle-left panel, the meander ratio was computed from original trajectories. For unM macrophages, it is higher than for M1-like and NonM1-like and more closely resembles that of M2-like, indicating more curved and less directed trajectories. The bottom-left and top-right panels show results for two features capturing random-like movement: r_{len}, representing the proportion of a trajectory's length involved in self-intersecting trajectories, and r_{seg}, representing the proportion of time spent in such patterns. Both measurements are significantly higher in unM macrophages than in M1-like and NonM1-like, and are similar to M2-like values, further indicating a predominance of random patterns of circuitous motion. Despite these similarities with M2-like macrophages, unM macrophages also exhibit distinct features, as shown in the middle- and bottom-right panels. In the middle-right panel, unM macrophages show the highest mean circularity among all modes, indicating the most rounded morphology, in contrast to the highly elongated shapes observed in M2-like macrophages. Furthermore, in the bottom-right panel, unM macrophages exhibit the lowest median of speed (computed from original trajectories) among all activation states, suggesting a relatively inactive or weakly migratory state.

Discussion

In this study, we investigated distinct behavioral modes of macrophages during wound healing in a zebrafish model. Using a comprehensive analysis pipeline, we computed 63 morpho-kinetic features to characterize macrophage behavior in a high-dimensional feature space (see Supplementary Information, Supplementary Fig. 8, for the full analytic workflow).

We quantitatively compared M1-like and M2-like macrophages across several aspects, including morphology, movement directionality, proximity to the wound, and trajectory shape. Our results showed that M2-like macrophages are more elongated, exhibit less directed migration toward the wound (and in some cases reverse migration), maintain higher meander ratios (indicating circuitous paths), and tend to remain farther from the wound site. These findings suggest that M2-like macrophages may be responding to a weaker or diminishing chemoattractant signal, resulting in less targeted movement toward the wound.

Using the features extracted from annotated M1-like and M2-like data, we classified macrophage trajectories from the transitional period (6–10.5 h post-amputation, hpa) into cM1-like or cM2-like groups. The classification indicates that the cM1-like and cM2-like groups closely resembled the annotated M1-like and M2-like trajectories, respectively, in terms of morpho-kinetic properties averaged over the observation period for each trajectory. The extracted trajectories during the transition period (TP) originate from macrophages that have been or are currently expressing the tnfa:GFP-f transgene. The classifier was trained to distinguish only between cM1-like and cM2-like behaviors based on these average features within the TP; therefore, the assigned labels reflect the dominant phenotype of each trajectory rather than the timing of the M1-like-to-M2-like switch. As a result, some trajectories classified as cM1-like may exhibit cM2-like behavior in the later part of the TP, while some cM2-like trajectories may include cM1-like behavior in the early part of the TP. To better capture the temporal dynamics of the M1-like-to-M2-like transition, we analyzed the classified groups by dividing their trajectories into time bins (Fig. 2B,C). This allowed us to investigate temporal patterns of morpho-kinetic behavior within each group, providing a more detailed view of their dynamic changes over time. With this temporal analysis of the classified cM1-like and cM2-like groups, we were able to estimate the approximate timing of the M1-like-to-M2-like shift. The cM2-like macrophages begin to show TPM values $\leq$ 0 (indicating loss of directed movement toward the wound) around 460 minutes post-amputation (mpa), with reverse migration observed after 550 mpa. Therefore, the time range of 460-550 mpa likely corresponds to the point at which M1-like macrophages begin transitioning to the M2-like mode. Moreover, pairwise feature

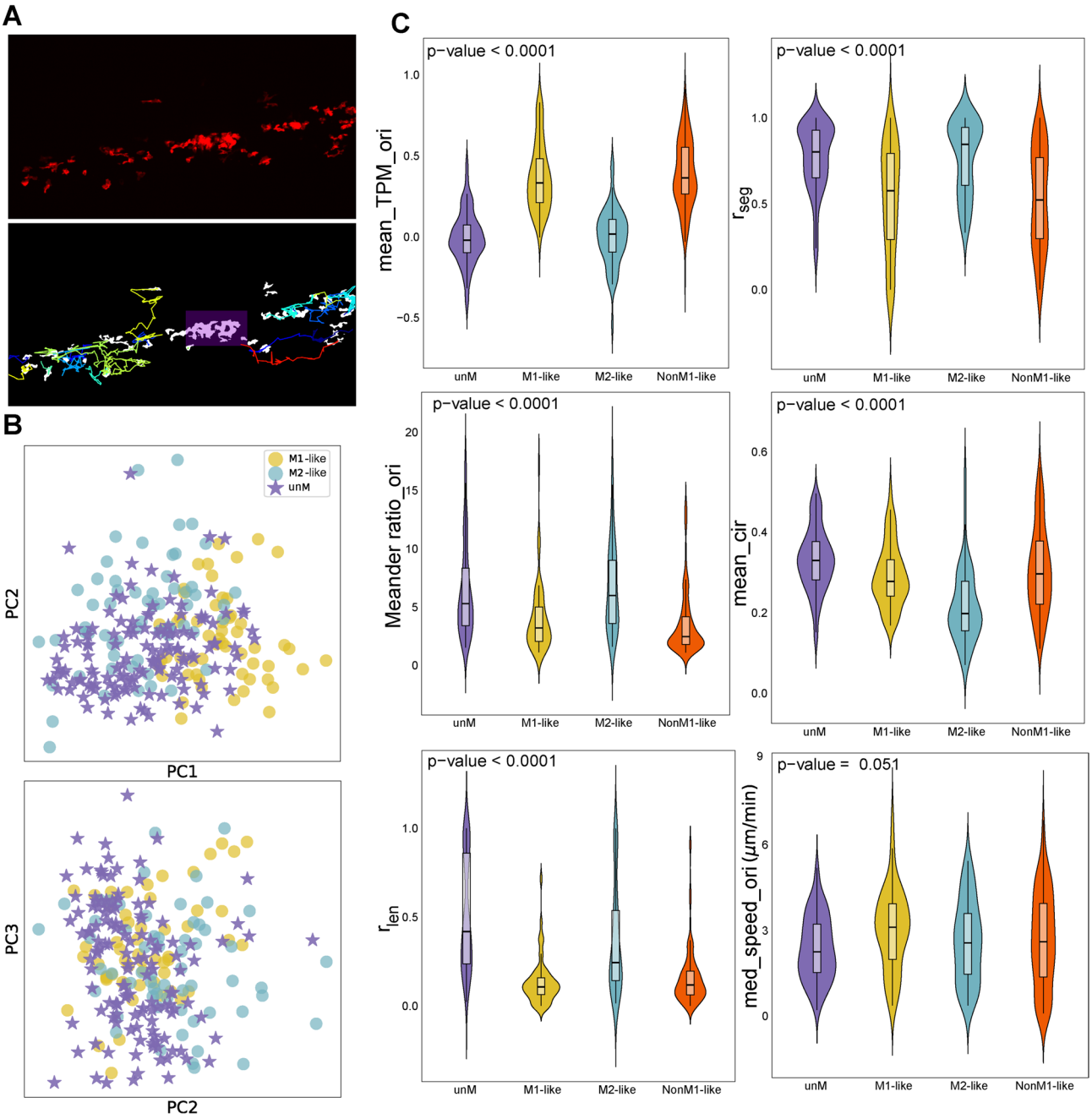

Figure 4. Morpho-kinetic analysis of unM macrophages in the absence of wound signal. (**A**) Examples of macrophage segmentation and tracking from an annotated unM video. The top panel shows an original image at a single time frame (with red channel). The bottom panel shows the result after macrophage segmentation and tracking of unM macrophages, where segmented macrophages are displayed in white and individual trajectories are color-coded. Transparent violet regions (bottom) indicate manually defined macrophage accumulation zones. (**B**) Projection of unM trajectories onto the PCA planes derived from labeled M1-like and M2-like macrophages. (**C**) Comparison of unM and other macrophage modes across all videos of each mode for selected features: mean Tangent Projection Metric (top-left panel; mean_TPM_ori; positive values indicate movement toward the wound, negative values away from it), proportion of random-like motion in terms of time frames (top-right; r_{seg}), meander ratio (middle-left; Meander ratio_ori), mean circularity of cell shapes (middle-right; mean_cir), proportion of random-like motion in terms of trajectory length (bottom-left; r_{len}), and median speed (bottom-right; med_speed_ori). Abbreviations for the feature names are described in detail in the Supplementary Information. Features with the "ori" suffix were computed from original (unsmoothed) trajectories.

analysis revealed that cM2-like macrophages exhibit increased speed and elongation during reverse migration, providing further insight into the dynamics of this shift.

We also analyzed NonM1-like macrophages that do not express TNF. Although most NonM1-like macrophages clustered near M1-like macrophages in the PCA planes based on morpho-kinetic features, they exhibited a significantly greater distance to the wound, indicating that they were located farther away. This suggests that TNF transcriptional activation, indicated by tnfa:GFP-f expression, is spatially associated with wound proximity. Finally, we examined unM macrophages (those not exposed to wound signals). These macrophages displayed no clear directionality, exhibited similar patterns of random-like movement to M2-like macrophages, but maintained high circularity and low speed, indicating a rounded and minimally migratory phenotype.

Collectively, in the context of wound healing, our study measures 63 morpho-kinetic features encompassing both morphological properties (such as shape descriptors) and kinetic behaviors (including trajectory characteristics, directional versus random-like motion patterns, and spatial dynamics relative to the wound). This comprehensive feature set, combined with automated classification methods, enabled us to characterize distinct macrophage modes, estimate the timing of phenotypic transitions, and establish a quantitative framework for analyzing macrophage behavior during wound healing *in vivo*.

Recent *in vivo* studies have demonstrated that morphological parameters and motility measurements can provide quantitative descriptors of macrophage functional states. One study showed that morphological parameters measured over time can differentiate resident tissue macrophages in response to chemical activation[25]. Another study examining speed and circularity over time revealed that macrophages of the same activation state but with distinct morphologies can exhibit similar functional behaviors, highlighting the complex relationship between form and function[26]. Complementing these *in vivo* findings, several *in vitro* studies have explored macrophage classification using morphology and movement. For example, in a study using primary murine bone marrow-derived macrophages[27], cells were maintained in the unM state, or polarized toward M1-like or M2-like states, and they were tracked under time-lapse imaging. A deep learning model trained only on cell trajectories achieved over 90% classification accuracy, demonstrating that kinetic patterns are informative for distinguishing macrophage modes. Also, the authors interpreted characteristic migratory behaviors for each macrophage subtype e.g., unM macrophages were described as "jiggling in place", which is consistent with our observation of low-motility unM macrophages *in vivo*. Another study focused on morphological features, using macrophages differentiated from human monocytes[28]. The authors extracted shape descriptors (area, eccentricity, etc.) and were able to classify M1-like and M2-like cells, and distinguish them from naive macrophages and monocytes, with approximately 90% accuracy. This indicates that cell morphology differs significantly between polarization states and can be used as significant features to distinguish them. In addition, a study using two-photon fluorescence lifetime imaging (2P-FLIM) on human macrophages[29] demonstrated that M1-like and M2-like macrophages exhibit distinct metabolic dynamics. By analyzing fluorescence lifetime parameters reflecting metabolic activity and applying a random forest classifier, an accuracy score up to 0.94 was achieved. This work highlights that metabolic behavior, similarly to motility and morphology, is a discriminative feature of macrophage polarization. These studies collectively demonstrate that macrophage polarization differs not only in gene expression, but also in morphological, kinetic, and metabolic characteristics, implying that each of these can be used as a key descriptor for classification.

Our study opens several directions for future research. The development of a method to register identical cells between the red channel (mfap4:mCherry-F) and green channel (tnfa:GFP-f) would enable analysis of the exact timing of macrophage activation and reveal the relationship between activation timing and spatial positioning. In addition, advanced multi-dimensional interpretation methods that reveal complex interactions among multiple features simultaneously could provide additional insights into macrophage behavior across modes. Our study employed multi-dimensional analyses using all 63 morpho-kinetic features, including PCA-based dimensionality reduction in 6-dimensional space and automated classification during the transition period, to capture the full behavioral landscape of each macrophage mode. For interpretability and clarity, we presented results by examining individual or pairwise features to highlight specific behavioral characteristics that distinguish each mode. Future studies could complement this approach with methods that quantify and visualize feature interactions, potentially revealing emergent behavioral signatures not apparent from individual feature analysis. Lastly, we classified cM1- and cM2-like trajectories during the TP using a classifier with 90.4% accuracy and analyzed their temporal behavioral differences based on the classified trajectories. Although this approach can estimate the timing of phenotypic switching (from M1-like to M2-like), finer temporal resolution would enhance our understanding of the behavioral changes during switching. Because our method computed five statistics (mean, median, standard deviation, minimum, maximum) for each trajectory over its entire duration, it captures overall behavioral patterns rather than precise transition dynamics. To achieve finer temporal resolution, future approaches could develop classifiers capable of operating on shorter trajectory segments, allowing individual trajectories to be split into time windows and each segment classified independently. Additionally, methods that incorporate temporal information directly into the feature set, or employ soft clustering to identify intermediate phenotypes, could better capture gradual transitions. These approaches would enable more precise estimation of when individual macrophages undergo phenotypic switching, providing deeper insights into the dynamics of macrophage behavioral transitions during wound healing.

Materials and methods

Ethics statement

Fish husbandry, embryo collection and animal experiments were conducted by well-trained and authorized staff at LPHI laboratory (CNRS/UMR5294), University of Montpellier, according to European Union guidelines for handling of laboratory animals (https://ec.europa.eu/environment/chemicals/lab_animals/index_en.htm) and

were approved by the Comité d'Ethique pour l'Expérimentation Animale under reference CEEA-LR- B4-172-37. Developmental stages used were between 3 days post-fertilization (dpf) and 4 dpf. Specimens were euthanized using an anesthetic overdose of buffered tricaine.

Study design

This study investigated the behavior of macrophages in zebrafish larvae following caudal fin fold amputation. Experimental units were individual larvae, randomly assigned to wounded or unwounded conditions. The primary comparison was between different macrophage phenotypes across time points after injury. Based on the acquired time-lapse image data, we performed a comprehensive quantitative analysis of macrophage morpho-kinetic behaviors. This manuscript complies with the ARRIVE guidelines 2.0. The corresponding checklist is provided in Supplementary Table 3.

Data acquisition and macrophage annotation

The datasets used in this study consist of *in vivo* videos of migrating macrophages in the tail region of transgenic Tg(mfap4:mCherry-F)ump6 ; Tg(tnfa:GFP-F)ump5 zebrafish larvae, at 3 dpf. To induce a wound response, larvae were first anaesthetized in zebrafish medium supplemented with 200 $\mu g/ml$ tricaine (ethyl 3-aminobenzoate methanesulfonate, MS-222 sigma # A5040). Then, the caudal fin fold was amputated with a sterile scalpel, posterior to muscle and notochord and larvae were either transferred in their medium at 28 $^{\circ}$C until later imaging or mounted in 1% low-melting point agarose approximately 20 minutes after amputation (to allow partial wound closure), as previously described[18]. Intra-vital imaging was performed using an ANDOR CSU-W1 confocal spinning disk on an inverted NIKON microscope (Ti Eclipse) with ANDOR Neo sCMOS camera (20x air/NA 0.75 objective); lasers 488 *nm* (GFP) and 561 *nm* (mCherry). Image stacks for time-lapse movies were acquired at 28 $^{\circ}$C with following setups: Time steps and time ranges are indicated in Supplementary Table 1, z step was 1 to 3 μm. Macrophages were identified by the expression of the mfap4:mCherry-F transgene, allowing the production of a membrane-localized red fluorescent protein indicating cell identity. M1-like activation of macrophages was identified by the expression of the tnfa:GFP-f transgene, allowing the production of a membrane-localized green fluorescent protein in cell producing TNF, a known marker of M1-like macrophages. For the analysis, 4D files generated from time-lapse acquisitions were projected into two dimensions using the maximum intensity projection. Macrophage behavior observed in the videos was annotated into four distinct modes, as detailed in Table 1 of the Supplementary Information. As no specific marker for M2-like macrophages was available in this experimental system, M1-like and M2-like annotations were assigned based on the time post-amputation, reflecting the time-dependent polarization from M1-like to M2-like states during wound healing in zebrafish. The annotation of macrophages considered both activation of the tnfa:GFP-f transgene and the time after amputation. M1-like expressed tnfa:GFP-f and were present during the first 6 hours post-activation (hpa), corresponding to the pro-inflammatory phase with macrophages up-regulating cytokines, chemokines and key pro-inflammatory pathways, meanwhile increasing levels of genes of glycolysis[24]. M2-like were defined as macrophages transitioning from M1-like, observed between 10.5 and 16 hpa, a time window corresponding to inflammation resolution; macrophages from this period are known to down-regulate pro-inflammatory pathway while expressing metalloproteinases[24]. NonM1-like were macrophages that did not show TNF expression within the first 6 hpa; and unM were macrophages in homeostasis, without any wound. Additionally, macrophages showing TNF expressing during the transition period (6-10.5 hpa) were labeled as TP.

Sample size

A total of 10 zebrafish larvae were used in this study. Of these, 5 were used to study M1-like, NonM1-like, and TP modes. Among them, 3 were suitable for TP analysis based on the time window. Two larvae were used to study M2-like and TP states, and 3 unwounded larvae were used for the unM state. No formal sample size calculation was performed. The sample sizes were determined based on previous studies using similar experimental setups.

Randomisation, blinding, and inclusion criteria

Larvae were randomly assigned to experimental conditions (wounded or unwounded) from the same developmental batch without using a formal randomization procedure. Image annotation and macrophage classification were performed according to predefined criteria (time window and gene expression). M1-like and M2-like classification in the TP was performed entirely using a computational method without subjective input. No animals or data points were excluded unless imaging was incomplete or the larvae were damaged during mounting. These criteria were established prior to analysis.

Analysis methods

Statistical analyses were performed using R and Python. Group comparisons were tested using the Kruskal-Wallis test, followed by Bonferroni-adjusted Dunn's post hoc test. Moving average and pairwise spatial analyses were conducted in Python. All numerical methods for image segmentation, tracking, trajectory smoothing, and classification were implemented by us in C and C++.

Macrophage segmentation

Macrophage segmentation was performed using a multi-step workflow consisting of space-time filtering, local Otsu thresholding, and the Subjective Surface Segmentation (SUBSURF) method, as described in Park et al.[20].

Space-time filtering
Space-time filtering was applied to reduce noise while preserving macrophage signals by considering their temporal coherence. For a macrophage video with time slices on the interval $[0, \theta_F]$, where θ represents a particular time slice, the space-time filtering is governed by

$$\frac{\partial u}{\partial t} = clt(u)\nabla \cdot \big(g(|\nabla G_\sigma * u|)\nabla u\big). \tag{1}$$

Here, t represents the scale (amount of filtering) and $u(t, x_1, x_2, \theta)$ is the unknown real function defined on $[0, T_F] \times \Omega \times [0, \theta_F]$, with $\mathbf{x} = (x_1, x_2) \in \Omega \subset R^2$. The *clt*(*u*) function is defined as[30]

$$clt(u) = \min_{\boldsymbol{w_1}, \boldsymbol{w_2}} \frac{1}{(\Delta\theta)^2}\big(| < \nabla u, \boldsymbol{w_1} - \boldsymbol{w_2} > | + |u(\mathbf{x} - \boldsymbol{w_1}, \theta - \Delta\theta) - u(\mathbf{x}, \theta)| + |u(\mathbf{x} + \boldsymbol{w_2}, \theta + \Delta\theta) - u(\mathbf{x}, \theta)|\big), \tag{2}$$

where $\boldsymbol{w}_1$ and $\boldsymbol{w}_2$ are arbitrary vectors in 2D space, $\Delta\theta$ is the time increment between discrete time slices, and $< \boldsymbol{a}, \boldsymbol{b} >$ denotes the Euclidean scalar product. The edge detector function *g* is defined as

$$g(s) = \frac{1}{1 + Ks^2}, \ K > 0, \tag{3}$$

where *K* controls the sensitivity to *s*. G_σ is a Gaussian function with variance σ used for pre-smoothing by convolution.

Local otsu thresholding
After filtering, we applied the local Otsu's method to identify approximate macrophage regions by adaptively calculating thresholds for each pixel. The resulting binarized images were obtained based on

$$B(i,j) = \begin{cases} 1, I(i,j) > T^*_{i,j} \text{ and Equation 5 is fulfilled} \\ 0, \text{otherwise,} \end{cases} \tag{4}$$

$$\frac{|\mu_0(T^*_{i,j}) - \mu_1(T^*_{i,j})|}{\mu_0(T^*_{i,j})} > \delta, \tag{5}$$

where *I*(*i*, *j*) is the image intensity of a pixel (*i*, *j*). The optimal threshold $T^*_{i,j}$ maximizes the between-class variance

$$\begin{aligned} \sigma^2_B(T^*_{i,j}) &= \max_{0 \le T_{i,j} < L} \sigma^2_B(T_{i,j}), \\ \sigma^2_B(T_{i,j}) &= \frac{\big(\mu_{\text{tot}}\omega_0(T_{i,j}) - \mu_0(T_{i,j})\omega_0(T_{i,j})\big)^2}{\omega_0(T_{i,j})\big(1 - \omega_0(T_{i,j})\big)}, \end{aligned} \tag{6}$$

with the following terms defined as

$$\omega_0(T_{i,j}) = \sum_{r=0}^{T_{i,j}} p_r, \quad \mu_0(T_{i,j}) \quad = \frac{1}{\omega_0(T_{i,j})} \sum_{r=0}^{T_{i,j}} rp_r, \quad \mu_{\text{tot}} = \sum_{r=0}^{L} rp_r, \tag{7}$$

where p_r is the probability of intensity *r* in the local gray-level histogram, calculated as $p_r = n_r/N$, with n_r being the number of pixels with intensity *r* and *N* the total number of pixels in the local window.

Subjective surface segmentation (SUBSURF)
To refine macrophage boundaries and remove residual noise, the SUBSURF method[31] was applied to each 2D frame independently. The SUBSURF method is described by

$$\frac{\partial u}{\partial t} = |\nabla u|\nabla \cdot \left(g\frac{\nabla u}{|\nabla u|}\right), \tag{8}$$

where *u* is a level set function, $g = g\,(|\nabla G_\sigma * I_0|)$ as previously defined, and I_0 denotes the original image. The SUBSURF equation was solved for *u*(*t*, *x*) with $(t, x) \in [0, T_S] \times \Omega$, where $\Omega \subset \mathbb{R}^2$.

Parameter settings and post-processing
All segmentation parameters followed those in the original article[20], except for δ in the local Otsu thresholding. Specifically, the parameter δ was set to 0.4 for M1-like and TP videos, 0.3 for unM videos, and 0.5 for M2-like videos. As a post-processing step, we applied a weighted dilation and erosion approach[32] to complete fragmented macrophage segments, described by

$$\frac{\partial u}{\partial t} \pm v_{i,j}|\nabla u| = 0, \tag{9}$$

where $v_{i,j} = \frac{1}{2}(\tilde{S}_{i,j} + I_{i,j})$, with ± denoting erosion (+) and dilation (–), and $\tilde{S}_{i,j} = 1 - |I_{i,j} - T^*_{i,j}|$. This process involved 10 iterations each of dilation and erosion across all videos.

Segmentation of NonM1-like macrophages

Identification of NonM1-like macrophages, those present in mfap4:mCherryF (red channel) but lacking tnfa:GFP-f (green channel) activation, was performed by segmenting both green and red fluorescence channels using the same procedure, Eqs. (1)–(9). The red channel used a threshold parameter $\delta = 0.3$, with all other parameters matching those of the green channel (M1-like videos). NonM1-like macrophages were then detected by assessing the overlap between segmented regions in the red and green channels across all time frames. Segmented macrophages that were present exclusively in the red channel, without any corresponding overlap in the green channel, were annotated as NonM1-like. A detailed overview of this process is illustrated in Supplementary Fig. 1 of the Supplementary Information.

Macrophage tracking

Approximated centers and trajectory extraction

For tracking, we followed the approach outlined in Park et al.[20]. The process began by computing the approximated center of each macrophage through the solution of the Eikonal equation from the boundary of segmented regions.

$$\begin{aligned} |\nabla d(\mathbf{x})| &= 1, \qquad \mathbf{x} \in \Omega, \\ d(\mathbf{x}) &= 0, \qquad \mathbf{x} \in \partial\Omega, \end{aligned} \tag{10}$$

where Ω denotes a segmented macrophage, $\partial\Omega$ is its boundary, and $|\cdot|$ is the Euclidean norm in $\mathbb{R}^2$. The center was defined as the pixel with the maximum distance to the boundary (i.e., the most interior point). Next, partial trajectories were extracted from temporally overlapping segmented macrophages. These trajectories were then connected based on the direction of movement. To determine whether two partial trajectories should be connected, we estimated the cell center position $\mathbf{r}_{\mathrm{es}}$ just before or after the endpoint of a trajectory by extrapolating its path using the local slope, representing the direction of motion. A connection was established if the estimated point was sufficiently close to the endpoint $\mathbf{r}_{\mathrm{e}}$ of another trajectory, satisfying the condition:

$$|\mathbf{r}_{\mathrm{es}} - \mathbf{r}_{\mathrm{e}}| \leq \Delta r. \tag{11}$$

Additionally, connections were evaluated based on whether the estimated center $\mathbf{r}_{\mathrm{es}}$ was located near the start or end point of another trajectory across multiple consecutive time frames. Two trajectories were connected if both of the following conditions were satisfied.

$$|\mathbf{r}_{\mathrm{es}} - \mathbf{r}_{\mathrm{j}}| \leq \Delta r_2 \text{ and } \Theta_c \leq \Delta r_\theta, \tag{12}$$

where $\mathbf{r}_{\mathrm{j}}$ represents another trajectory close to the estimated point $\mathbf{r}_{\mathrm{es}}$, and Θ_c denotes the number of common time frames between trajectories considered for connection. For all videos analyzed in this study, we set $\Delta r_\theta = 5$. The spatial connection parameters Δr and Δr_2 were adjusted depending on the video type. For M1-like macrophages, we set $\Delta r = 60$ and $\Delta r_2 = 120$. For M2-like macrophages, NonM1-like macrophages, and unM macrophages, we used $\Delta r = 50$ and $\Delta r_2 = 100$. For TP videos, we employed intermediate values with $\Delta r = 55$ and $\Delta r_2 = 110$. All remaining parameters were maintained as reported in the original method[20]. To ensure robustness in tracking, only segmented regions with a maximum distance from the boundary greater than 6.5 were considered, thereby excluding minor segmented regions.

Exclusion of short and unreliable trajectories

To ensure reliable analysis, only trajectories with a sufficient number of time points, corresponding to at least one hour of continuous movement, were considered. For example, in videos with a temporal resolution of 2.5 minutes per frame, only trajectories containing more than 24 points were included. Additionally, due to macrophage accumulation at wound sites, the 2D projection of the data can result in the visual merging of adjacent macrophages. This often leads to segmentation artifacts, where multiple cells appear as a single connected region, potentially leading to inaccurate trajectory interpretation. To mitigate this issue, we manually defined a macrophage accumulation zone (MAZ), indicated by violet rectangles in Fig. 2 of the Supplementary Information. Trajectory segments in which macrophages remained within an MAZ for more than five consecutive time frames were excluded from further analysis.

Trajectory smoothing and randomness extraction

To separately analyze directional and random-like macrophage motion, we applied the trajectory smoothing model proposed by Lupi et al.[21], extracting segments of the random-like motion. This method is based on evolving curves, formulated through the following partial differential equation.

$$\frac{\partial \mathbf{x}}{\partial t} = -\delta(\mathbf{x}, t) k \mathbf{N} + \lambda(\mathbf{x}, t) \left[(\mathbf{x}_0 - \mathbf{x}) \cdot \mathbf{N}\right] \mathbf{N} + \alpha \mathbf{T}. \tag{13}$$

This equation describes the evolution of points $\mathbf{x}$ along the curve through three key components: a curvature-based smoothing term, $-k\mathbf{N}$ that depends on the local curvature k; an attracting term, $[(\mathbf{x}_0 - \mathbf{x}) \cdot \mathbf{N}]\mathbf{N}$ that preserves the shape of the original trajectory; and a tangential component, $\alpha\mathbf{T}$ for numerical stability, where

$\mathbf{T}$ and $\mathbf{N}$ denote the unit tangent and normal vectors, respectively. In this model, the parameters $\delta(\mathbf{x}, t)$ and $\lambda(\mathbf{x}, t)$ were adaptively selected based on the presence of self-intersections along the curve, and thus depend on both spatial and temporal coordinates. Trajectory segments that lie within self-intersecting regions were specifically targeted for smoothing. These segments, referred to as random segments, are defined as portions of the trajectory between two self-intersection points, including all intermediate points.

Extraction of morpho-kinetic features

After the aforementioned processing steps, we computed both morphological and kinetic features for individual macrophages from extracted trajectories.

Morphological features were computed from the segmented regions (i.e., connected regions) containing each trajectory point and were analyzed along the full trajectories over time. For simplicity, we refer to these regions as segmented macrophages; they were derived from binarized images obtained through the segmentation workflow. For each segmented macrophage, we computed the area, perimeter, and circularity across all time frames. Circularity quantifies the roundness of a shape, where a value of 1 corresponds to a perfect circle. Lower circularity values indicate more elongated or irregular morphologies, capturing greater structural complexity.

Kinetic features focused on four main aspects: trajectory shape, directionality toward the wound, distance to the wound, and speed. Trajectory shape was characterized using both extracted random segments and the meander ratio. Directionality was evaluated by projecting tangent and velocity vectors at each time frame onto the normal vector of the wound site. Distance to the wound was defined as the shortest distance to the macrophage's current position to the wound boundary. Speed was calculated across all time frames for each trajectory.

The detailed mathematical formulations are described in the Supplementary Information, along with an overview of these features (Table 2).

Classification of macrophage trajectories

To analyze macrophage behavior during the transition period, we classified M1- and M2-like trajectories (cM1-like and cM2-like, respectively) based on extracted morpho-kinetic features. For this, we used *NatNet*[22], a nonlinear graph-diffusion classifier that operates in a reduced feature space. The model was trained using annotated data consisting of trajectories labeled as M1-like or M2-like, with morpho-kinetic features computed for each trajectory. Optimal model parameters were determined during the training process. After identifying the optimal parameters, the classifier was applied to trajectories from the transition period to assign cM1-like or cM2-like labels based on their similarity to the annotated trajectories. Classification is performed by solving the graph diffusion equation, as described below.

$$\frac{\partial X(v,t)}{\partial t} = \nabla \cdot (g \nabla X(v,t)), \quad v \in V(G), \quad t \in [0,T] \tag{14}$$

In this equation, $X : G \times [0,T] \to \mathbb{R}^k$ represents the Euclidean coordinates of vertex $v \in V(G)$ at time t, where t is an abstract time variable associated with the graph diffusion process, with $X(v,t) = (x_1(v,t), \ldots, x_k(v,t))$ and k being the dimensionality of the reduced feature space $\mathbb{R}^k$. The equation models a diffusion process over the directed graph G.

The diffusion coefficient g associated with an edge e_{uv} is defined as

$$g(e_{uv}) = \frac{\varepsilon(e_{uv})}{1 + \sum_{i=1}^{k} K_i l_i^2(e_{uv})}, \quad K_i \geq 0, \quad i = 1, \ldots, k, \tag{15}$$

where $\varepsilon(e_{uv})$ depends on the type of diffusion. For edges connecting nodes of the same class, $\varepsilon(e_{uv})$ is positive and represents the forward diffusion that attracts the nodes to each other (typically set to 1). For edges between nodes of different classes, $\varepsilon(e_{uv})$ is assigned a small negative value, representing the backward diffusion that repels the nodes.

Here, K_i are weights assigned to each coordinate $l_i(e_{uv})$ of the vector, $l(e_{uv}) = (l_1(e_{uv}), \ldots, l_k(e_{uv}))^\top = X(v,\cdot) - X(u,\cdot) = (x_1(v,\cdot) - x_1(u,\cdot), \ldots, x_k(v,\cdot) - x_k(u,\cdot))^\top$ for $u, v \in V(G)$.

The accurate classification relies on appropriately tuning the parameters of the diffusion coefficient g, particularly the weights K_i. Once optimal parameters are determined, new nodes (trajectories) can be added to the graph and classified by propagating them through the optimized graph diffusion network. For any new trajectory, $\varepsilon(e_{uv})$ is set to a positive value such that it is attracted to all nodes of the directed graph, and it is then assigned to the class with which it is most closely associated according to the network dynamics[23].

To reduce the dimensionality of the original 63-dimensional feature space, we applied principal component analysis (PCA). We selected the first 6 principal components, as the eigenvalues beyond the 6th component were small and nearly uniform (see Fig. 2A). The final classification, therefore, was conducted in this reduced 6-dimensional PCA space by solving Eq. (14).

The optimal diffusion coefficient g was determined using trajectories from annotated videos based on the time period after amputation, each representing either an M1-like or M2-like trajectory. Morpho-kinetic features from the TP videos were extracted, and trajectories in the TP were then classified by NatNet as cM1-like or cM2-like. In this study, the optimal parameters K_i, for $i = 1, \ldots, 6$ in Eq. (15) were obtained as follows: $K_1 = 4050$, $K_2 = 3800$, $K_3 = 50$, $K_4 = 550$, $K_5 = 3300$, and $K_6 = 2800$.

Data availability

The raw imaging and processed datasets containing extracted macrophage trajectories and morphological features are available at Zenodo: 10.5281/zenodo.16319732

Received: 25 July 2025; Accepted: 14 January 2026
Published online: 28 January 2026

References

1. Sonnemann, K. J. & Bement, W. M. Wound repair: toward understanding and integration of single-cell and multicellular wound responses. *Ann. Rev. Cell Develop. Biol.* **27**, 237–263 (2011).
2. Wynn, T. A., Chawla, A. & Pollard, J. W. Macrophage biology in development, homeostasis and disease. *Nature* **496**, 445–455 (2013).
3. Hesketh, M., Sahin, K. B., West, Z. E. & Murray, R. Z. Macrophage phenotypes regulate scar formation and chronic wound healing. *Int. J. Mol. Sci.* **18**, 1545 (2017).
4. Benoit, M., Desnues, B. & Mege, J.-L. Macrophage polarization in bacterial infections. *J. Immunol.* **181**, 3733–3739 (2008).
5. Daley, J. M., Brancato, S. K., Thomay, A. A., Reichner, J. S. & Albina, J. E. The phenotype of murine wound macrophages. *J. Leukoc. Biol.* **87**, 59–67 (2010).
6. Lucas, T. et al. Differential roles of macrophages in diverse phases of skin repair. *J. Immunol.* **184**, 3964–3977 (2010).
7. Koh, T. J. & DiPietro, L. A. Inflammation and wound healing: the role of the macrophage. *Expert Rev. Mol. Med.* **13**, e23 (2011).
8. Friedl, P. & Weigelin, B. Interstitial leukocyte migration and immune function. *Nat. Immunol.* **9**, 960–969 (2008).
9. Van Goethem, E., Poincloux, R., Gauffre, F., Maridonneau-Parini, I. & Le Cabec, V. Matrix architecture dictates three-dimensional migration modes of human macrophages: differential involvement of proteases and podosome-like structures. *J. Immunol.* **184**, 1049–1061 (2010).
10. Barros-Becker, F., Lam, P.-Y., Fisher, R. & Huttenlocher, A. Live imaging reveals distinct modes of neutrophil and macrophage migration within interstitial tissues. *J. Cell Sci.* **130**, 3801–3808 (2017).
11. Cui, K., Ardell, C. L., Podolnikova, N. P. & Yakubenko, V. P. Distinct migratory properties of m1, m2, and resident macrophages are regulated by αdβ2 and αmβ2 integrin-mediated adhesion. *Front. Immunol.* **9**, 2650 (2018).
12. Adebowale, K. et al. Monocytes use protrusive forces to generate migration paths in viscoelastic collagen-based extracellular matrices. *Proc. Natl. Acad. Sci.* **122**, e2309772122 (2025).
13. Mosser, D. M. & Edwards, J. P. Exploring the full spectrum of macrophage activation. *Nat. Rev. Immunol.* **8**, 958–969 (2008).
14. Strizova, Z. et al. M1/m2 macrophages and their overlaps-myth or reality?. *Clin. Sci.* **137**, 1067–1093 (2023).
15. Ghamangiz, S., Jafari, A., Maleki-Kakelar, H., Azimi, H. & Mazloomi, E. Reprogram to heal: Macrophage phenotypes as living therapeutics. *Life Sci.* 123601 (2025).
16. Nguyen-Chi, M. et al. Identification of polarized macrophage subsets in Zebrafish. *Elife* **4**, e07288 (2015).
17. Miskolci, V. et al. Distinct inflammatory and wound healing responses to complex caudal fin injuries of larval zebrafish. *Elife* **8**, e45976 (2019).
18. Sipka, T. et al. Macrophages undergo a behavioural switch during wound healing in Zebrafish. *Free Radical Biol. Med.* **192**, 200–212 (2022).
19. Crainiciuc, G. et al. Behavioural immune landscapes of inflammation. *Nature* **601**, 415–421 (2022).
20. Park, S. A. et al. Segmentation-based tracking of macrophages in 2d+ time microscopy movies inside a living animal. *Comput. Biol. Med.* **153**, 106499 (2023).
21. Lupi, G. et al. Mathematical and numerical methods for understanding immune cell motion during wound healing. *Math. Model. Nat. Phenomena* **20**, 28 (2025).
22. Mikula, K. et al. Natural numerical networks for natura 2000 habitats classification by satellite images. *Appl. Math. Model.* **116**, 209–235 (2023).
23. Mikula, K., Kollár, M., Ožvat, A. A., Šibíková, M. & Čahojová, L. Natural numerical networks on directed graphs in satellite image classification. In *International Conference on Scale Space and Variational Methods in Computer Vision*, 339–351 (Springer, 2023).
24. Begon-Pescia, C. *et al.* Temporal dynamics of macrophages transcriptional profiles during zebrafish wound healing. *Frontiers in Immunology* **16**,1721612 (2026).
25. Schnitzerlein, M. et al. Cellular morphodynamics as quantifiers for functional states of resident tissue macrophages in vivo. *PLoS Comput. Biol.* **21**, e1011859 (2025).
26. Paterson, N. & Lämmermann, T. Macrophage network dynamics depend on haptokinesis for optimal local surveillance. *Elife* **11**, e75354 (2022).
27. Kesapragada, M. et al. Deep learning classification for macrophage subtypes through cell migratory pattern analysis. *Front. Cell Develop. Biol.* **12**, 1259037 (2024).
28. Rostam, H. M., Reynolds, P. M., Alexander, M. R., Gadegaard, N. & Ghaemmaghami, A. M. Image based machine learning for identification of macrophage subsets. *Sci. Rep.* **7**, 3521 (2017).
29. Neto, N. G. et al. Non-invasive classification of macrophage polarisation by 2p-flim and machine learning. *Elife* **11**, e77373 (2022).
30. Sarti, A., Mikula, K. & Sgallari, F. Nonlinear multiscale analysis of three-dimensional echocardiographic sequences. *IEEE Trans. Med. Imaging* **18**, 453–466 (1999).
31. Sarti, A., Malladi, R. & Sethian, J. A. Subjective surfaces: A method for completing missing boundaries. *Proc. Natl. Acad. Sci.* **97**, 6258–6263 (2000).
32. Park, S. A. & Mikula, K. Automated completion of segmented fragments of macrophages using weighted dilation and erosion in 2d+ time microscopy videos. In *Proceedings of ALGORITMY*, 11–20 (2024).

Acknowledgements

We thank the Aquatic model facility ZEFIX from LPHI (University of Montpellier) and the imaging facility BioCampus Montpellier Ressources Imagerie (MRI), member of the national infrastructure France-BioImaging supported by the French National Research Agency (ANR-10-INSB-04, 'Investments for the future').

Author contributions

S.A.P. designed the analysis workflow, tested and performed the data analysis, and wrote the manuscript. G.L. contributed the method of trajectory smoothing and participated in discussions on designing the analysis workflow. R.O. acquired and provided the data and contributed to the biological interpretation of the results. M.K. and A.A.O. contributed the classification method. M.N.C. co-led the project, acquired and provided the data, and contributed to the biological interpretation. K.M. led the project, designed the analysis workflow, and co-wrote the manuscript.

Funding
This work has received funding from the European Union's Horizon 2020 research and innovation programme under the Marie Skłodowska-Curie ITN INFLANET: grant agreement No. 955576, as well as from grants APVV-23-0186, VEGA 1/0249/24, and VV-MVP-24-0116.

Declarations

Competing interests
The authors declare no competing interests.

Additional information
Supplementary Information The online version contains supplementary material available at https://doi.org/10.1038/s41598-026-36624-w.

Correspondence and requests for materials should be addressed to S.A.P.

Reprints and permissions information is available at www.nature.com/reprints.

Publisher's note Springer Nature remains neutral with regard to jurisdictional claims in published maps and institutional affiliations.